Nanoscale

PAPER

View Article Online
View Journal | View Issue

Cite this: *Nanoscale*, 2014, **6**, 12710

Anemone-like nanostructures for non-lithographic, reproducible, large-area, and ultra-sensitive SERS substrates†

Bihter Daglar,[a,b] Gokcen Birlik Demirel,[a,c] Tural Khudiyev,[a] Tamer Dogan,[a,d] Osama Tobail,[a,e] Sevde Altuntas,[f] Fatih Buyukserin[f] and Mehmet Bayindir*[a,b,d]

The melt-infiltration technique enables the fabrication of complex nanostructures for a wide range of applications in optics, electronics, biomaterials, and catalysis. Here, anemone-like nanostructures are produced for the first time under the surface/interface principles of melt-infiltration as a non-lithographic method. Functionalized anodized aluminum oxide (AAO) membranes are used as templates to provide large-area production of nanostructures, and polycarbonate (PC) films are used as active phase materials. In order to understand formation dynamics of anemone-like structures finite element method (FEM) simulations are performed and it is found that wetting behaviour of the polymer is responsible for the formation of cavities at the caps of the structures. These nanostructures are examined in the surface-enhanced-Raman-spectroscopy (SERS) experiment and they exhibit great potential in this field. Reproducible SERS signals are detected with relative standard deviations (RSDs) of 7.2–12.6% for about 10 000 individual spots. SERS measurements are demonstrated at low concentrations of Rhodamine 6G (R6G), even at the picomolar level, with an enhancement factor of ~10^{11}. This high enhancement factor is ascribed to the significant electric field enhancement at the cavities of nanostructures and nanogaps between them, which is supported by finite difference time-domain (FDTD) simulations. These novel nanostructured films can be further optimized to be used in chemical and plasmonic sensors and as a single molecule SERS detection platform.

Received 11th July 2014,
Accepted 15th August 2014

DOI: 10.1039/c4nr03909b

www.rsc.org/nanoscale

Introduction

The melt-infiltration technique enables the production of various materials on the nanoscale such as ceramics, alloys, metals, or polymers. In the simplest form, an active phase is infiltrated into a nanoporous template.[1] Nanorods, nanofibers, nanotubes, and ordered mesoporous materials are produced using this technique.[2–5] The main driving factors behind the formation of these structures are capillary forces, surface energies of the template/active phase, interface properties, and nanofluidics under the base of melt-infiltration.

Anodized aluminium oxide (AAO) and mesoporous silica materials are typical templates that are used in the melt-infiltration technique.[6,7] The wetting phenomenon is critical for the active phase and template interactions. Depending on wetting conditions, tubular or rod-like nanostructures can be produced.[8,9] The AAO template has several advantages compared to its silica counterparts. AAO has hexagonally packed ordered nanopores where the pore size and thickness can be arranged at desired dimensions. In addition, AAO is chemically inert under various conditions with a tremendous durability.[10]

AAO is widely used from drug loading studies to biosensing application owing to its advantages.[11,12] One of the benefits of AAO is observed in the convenience in using it for surface-enhanced Raman scattering (SERS) substrate production.[13–15] SERS enables analysis of a trace amount of chemical and biological molecules. Efforts to understand the precise mechanisms responsible for the SERS phenomenon are still insufficient to describe the underlying processes. However, there are two accepted independent proposals

[a]*UNAM-National Nanotechnology Research Center, Bilkent University, 06800 Ankara, Turkey. E-mail: bayindir@nano.org.tr*
[b]*Institute of Materials Science and Nanotechnology, Bilkent University, 06800 Ankara, Turkey*
[c]*Department of Chemistry, Gazi University, Polatli, 06900 Ankara, Turkey*
[d]*Department of Physics, Bilkent University, 06800 Ankara, Turkey*
[e]*Egypt Nanotechnology Center, Cairo University, 12588 Cairo, Egypt*
[f]*Department of Biomedical Engineering, TOBB University, 06560 Ankara, Turkey*

†Electronic supplementary information (ESI) available: SEM images of the AAO membrane and bare polymer film, FEM simulations of anemone-like polymeric nanopillars depending on the time and pressure, and detailed calculation of the enhancement factor both including experimental and theoretical approaches. See DOI: 10.1039/c4nr03909b

explaining the possible origin of enhancement: (i) electromagnetic enhancement and (ii) chemical enhancement.[16] Since electromagnetic enhancement is proportional to the fourth power of the electric field in SERS, it is assumed to take a major role in the enhancement factor. Excitation of the surface plasmons of metal nanostructures induces localized electric field enhancement. The inter-particle separation, size and shape of the nanostructures affect plasmon resonance and hence the SERS signal. In single-molecule detection studies, the enhancement factor is shown to be as high as $\sim 10^{14}$.[17,18] Typically, metallic nanoparticles are used in the single-molecule SERS studies.[19] In order to obtain high enhancement factors, inter-particle separation between plasmonic nanostructures is maintained at minimum values. However, proposed separations are not practical and the obtained signals are not reproducible.

As an alternative solution, periodic structures are fabricated to acquire large-area and reproducible SERS substrates.[20–22] Dar *et al*. proposed fabrication of tubular shaped metallic nanostructures using the AAO template and detected around 100 pM concentration.[23] Recently, Huang *et al*. reported silver coated silicon nanowire arrays. These ordered Ag/Si nanowire arrays show high reproducibility in the SERS detection due to their large interwire spacing with an enhancement factor of $\sim 10^6$.[24] Therefore, it is possible to fabricate reproducible and large-area SERS substrates using nanostructure arrays, but they all suffer from compromised enhancement factors.

In this work, we report fabrication of anemone-like nanopillars using the melt-infiltration technique *via* the AAO template. Formation of the nanostructures depends on the surface tension and capillary forces which were confirmed by COMSOL simulations. We can control the cap shape and heights of the nanostructures by tuning the fabrication conditions. We showed that silver coated anemone-like nanostructures provide exceptional electric field enhancement. According to FDTD simulations it was suggested that an enhanced electric field is mainly localized inside the cavity, which has a hole diameter of 40 nm; hence these structures can allow analysis of large and biological molecules. Utilizing these nanostructured features, we performed a set of SERS measurements and demonstrated that our nanostructures can be utilized as effective SERS substrates. Rhodamine 6G (R6G) was used to determine the SERS performance of anemone-like nanostructures and an enhancement factor of $\sim 10^{11}$ was experimentally obtained at the picomolar level. It is noteworthy that we obtained relative standard deviations (RSDs) of 7.2–12.6%, which implies that the reproducible signals were collected from 10 000 individual spots.

Results and discussion

Fabrication of anemone-like nanostructures

The melt-infiltration technique was used to produce anemone-like nanostructures. In this case, capillary effects, wetting, and viscosity are the main parameters influencing the infiltration of the active phase into the template. If the contact angle (Q) between the active phase and the template is smaller than 90°, the wetting process occurs spontaneously according to the Laplace equation (eqn (1)), where Δp is the capillary pressure difference, r_p is the pore radius, and γ_{lv} is the surface tension of the liquid.[25]

$$\Delta p = 2\gamma_{lv} \cos Q / r_p \quad (1)$$

In this study, polycarbonate (PC) was chosen as the polymeric material due to its durability, high impact resistance and wide usage in optics and electronics.[26] The AAO membrane was used as a template, supported on its aluminium substrate. Because PC is a reduced surface energy polymer, hydrophilic pores of the template were coated with fluorinated ligands in order to decrease the surface energy of the pore walls. Free AAO is fragile while the aluminium supported template is more durable and so much easier to handle. A PC film was placed on the AAO template and heated above its glass transition temperature step by step with no applied pressure. The polymeric film was easily peeled off from the template after cooling to room temperature (Scheme 1). Fabricated nanopillars had a cavity at their cap and resembled the sea anemone. The pillar height can be controlled by altering the

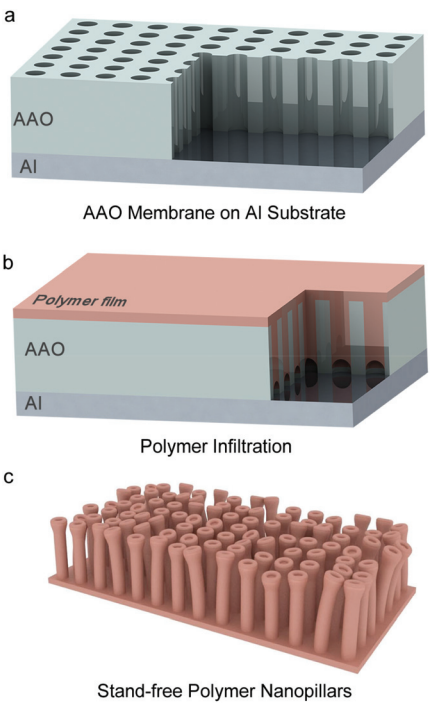

Scheme 1 Schematic representation of the anemone-like nanopillar fabrication process. (a) AAO membrane is supported on the aluminium substrate. (b) PC film is placed on the AAO template and heated over its glass transition temperature. Molten polymer wets the modified AAO pores relying on the surface interface properties. (c) Nanostructured film is peeled off from the template surface easily after the sample cools to room temperature. The schematic represents the fact that polymeric nanopillars are not oriented vertically and bend due to their soft nature.

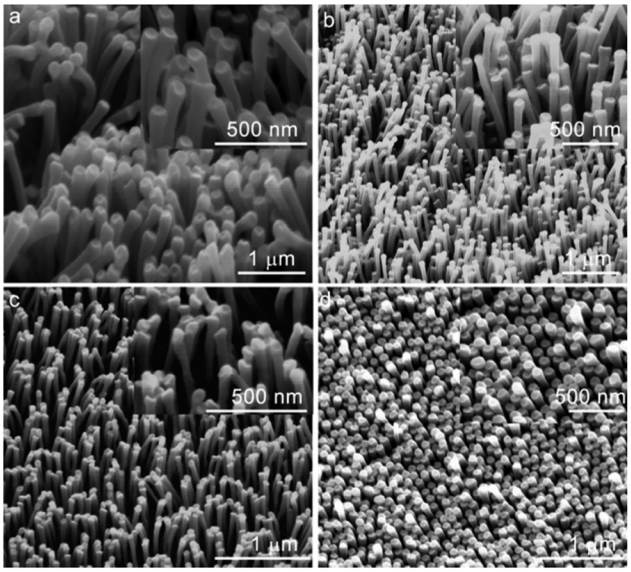

Fig. 1 SEM images of the nanopillars with a tilting angle of 40°. Nanopillars were produced at 215 °C at different durations (a) 1 h, (b) 30 min, (c) 15 min, and (d) 10 min. Insets show the higher magnification SEM images. Images demonstrate that the nanopillar height can be controlled with time, however the cavity of the nanopillars is not distinct for the pillars produced in 10 min.

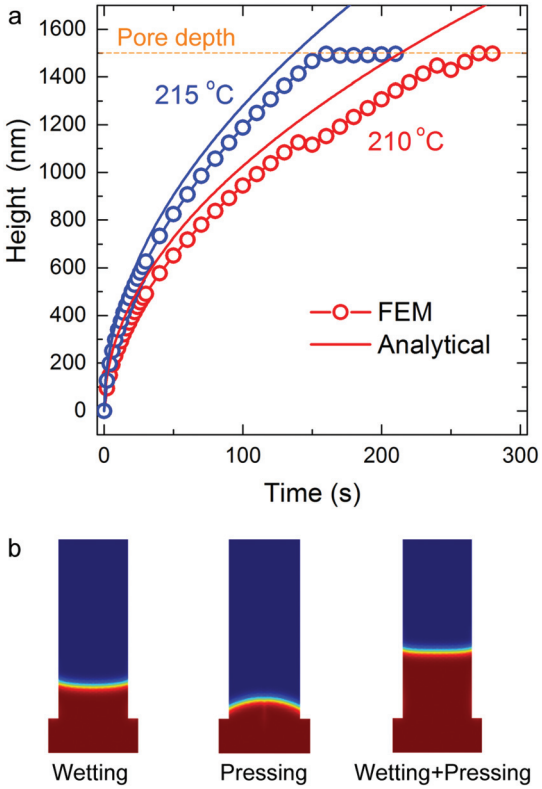

Fig. 2 Theoretical modelling of polycarbonate infiltration into the porous alumina template. (a) Comparison of FEM simulation and analytical calculation of polymer infiltration using the porous alumina template. The FEM simulation is consistent with analytical calculation especially at elevated temperatures, which is used in the experiment. (b) The interface profile dependence on the wetting, pressing and under both effects. The pillar head shape development is consistent with the experimental results in Fig. 1 and S4.† Red and blue regions respectively represent the polymer and air through the nanopore depth.

heating duration. The produced nanopillar heights varied from the nanometer to the micrometer scale (from 100 nm to 1–2 microns). SEM images of nanostructures with various lengths are given in Fig. 1. The area of the nanostructured surface depends on the large-area AAO membrane (ESI Fig. S1†).

To reveal the underlying mechanism of the formation of these anemone-like polymeric nanopillars, two dimensional numerical finite element method simulations (COMSOL) were performed. Our simulation models the infiltration of polymers, at elevated temperatures, based on the capillary penetration of the molten polymer, which is in direct contact with the porous alumina template (pores with 100 nm diameter and 1.5 μm depth). The polymer film acts as a reservoir of the molten polymer. Experimentally, it takes a considerably long time until the solid polymer absorbs the heat and melts depending on its specific heat capacity and latent heat. The straightforward problem of calculating the time needed until the polycarbonate melts depending on the heat diffusivities of the system components is out of the scope of this study, because it does not affect the shape of the nano-pillars.[27] Therefore, we describe the polymer as a fluid with a temperature dependent viscosity, which means that our simulation starts after a constant long time needed to melt the polymer in contact with the porous template.[28]

The polymer film was heated slowly until melting is observed. Modelled working temperatures are shown in Fig. 2a. Due to the axial symmetry of the system, we solve a time-dependent two dimensional axisymmetrical problem of two-phase fluid flow under the following forces: (1) the temperature dependent surface tension between the air and the polymer, (2) the temperature dependent wetting (contact angle) between the polymer and the pore-wall, which is experimentally determined (Q = 70° at $T \leq 200$ °C, Q = 50° $T >$ 200 °C), and finally (3) the pressure on the inlet, which is defined as the interface of the molten polymer and the solid polymer that was taken as zero except in the case of studying the effect of pressing on the nanopillar.[29] In the case where pressure was not applied, wetting was dominant and the polymer flowed *via* the template pores, which results in a cavity formation at the pillar caps (Fig. 2b and ESI Fig. S2†). Also, wetting, pressure and combination of these two effects are investigated. In the absence of wetting, pillar caps form a hemi-spherical shape. If we consider both of the effects simultaneously, we observe competition between the shapes which is also confirmed with the experimental findings (ESI Fig. S3 and S4†).

Theoretical simulations are compared with the analytical calculations in Fig. 2a. Capillary flow for a bundle of cylindri-

cal tubes with time (t) is given by Washburn's equation (eqn (2))

$$x(t) = \sqrt{\frac{r_p \gamma_{tv} \cos Q}{2\eta}}\sqrt{t} \quad (2)$$

where $x(t)$ is displacement of the liquid, r_p is the pore radius, $\cos Q$ is the contact angle of the liquid droplet on the surface, and η is the shear viscosity.[30] The working temperature should be considered because of the temperature-dependent character of the viscosity. The COMSOL simulation is consistent with analytical calculations especially at elevated temperatures used in the experiment (Fig. 2a).

We can clearly say that we can control both the cap shape and length of the nanopillars without using any kind of advanced patterning technique (e-beam lithography, photolithography, *etc.*). This production method can be adapted to different polymer types and utilized in various applications, such as plasmonic resonators, plasmonic or chemical sensors, gecko-like adhesive surfaces, drug loading or cell proliferation studies.

SERS performance

The controlled size and shape of anemone-like nanostructures are considered to be beneficial in SERS sensing application. Taller nanopillars, which were produced in ≥30 min (>1 micron), bend more than the shorter pillars due to their soft polymeric nature. The cavity at the caps of shorter nanopillars (<500 nm) is not distinct compared to taller structures, because the taller ones stay longer under the influence of the wetting effect. Therefore, to investigate the SERS feature of structured films, experimental studies were performed utilizing middle-height nanopillars produced in 15 min (~500–600 nm). Anemone-like nanostructures were coated with 40 nm silver using thermal evaporation. Two different AAO templates were used in the preliminary experiments with 75 nm and 100 nm pore sizes. After coating the produced nanopillars with silver, we observed that the cavity of nanopillars was completely filled in the case of the 75 nm pore sized template. For this reason, further experiments were carried out with a 100 nm pore sized AAO template.

As shown in Fig. 3, cavities of the pillars are conserved after 40 nm silver coating, although it is narrower than the initial state. Also, bead formation was observed throughout the pillars (Fig. S5†). For SERS sensing application, this bead formation turns into an advantage and they can behave like additional hot spots.[21]

To predict electric field enhancement and distribution in produced eccentric nanostructures, FDTD simulations were performed using the commercial software "Lumerical". Light metallic nanostructure interactions resulted in an enormous field enhancement on the metallic nanoparticle surface. The strength of this enhancement depends on the nanostructure shape and nanogaps between these structures. We examined dimensions of experimentally acquired anemone-like structures and the bead formation that occurred during thermal evaporation (Fig. 4a). In the case of the structure formation, the body of the pillar is formed of a polymer cylinder which is coated with a silver shell. Because bead formation was

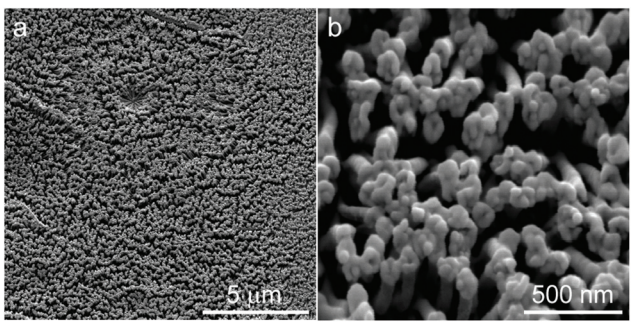

Fig. 3 SEM images of 40 nm silver coated anemone-like nanopillars. (a) After silver coating by thermal evaporation, the cavity of the nanopillars is still conserved and have a cavity with a diameter of ~40 nm. (b) Higher magnification image of the nanopillars.

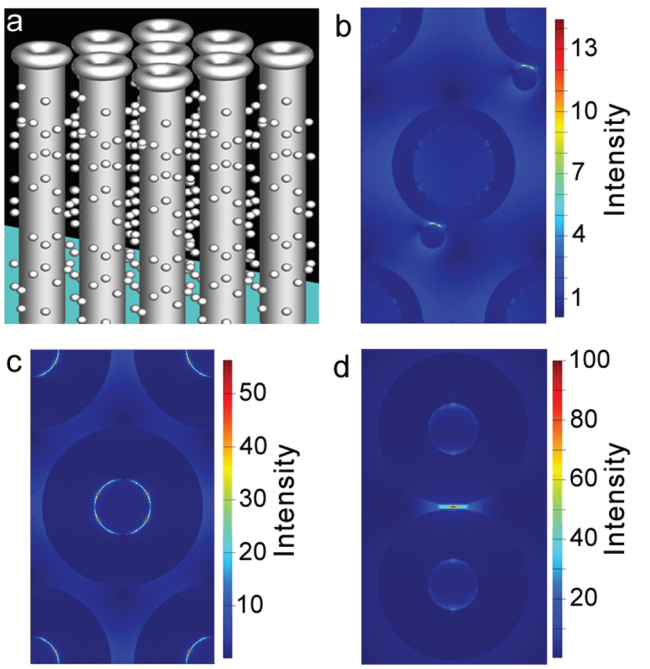

Fig. 4 FDTD simulation results. (a) Simulated anemone-like nanopillar structures are designed to appropriately reflect the experimentally obtained nanoarchitecture complexity (*i.e.* random nanobeads on body, anemone-like head). The possible origins of experimentally observed enormous enhancement values are explored by taking some critical points into consideration. (b) Interfaces of nanobeads and nanocylinders provide hot spots due to nanogaps but found to stay at the low intensity level (EF = 10^4–10^5). (c) However the anemone-like cap described as toroid geometry in our case was proven to supply field enhancement as high as 10^7. (d) Furthermore, according to "voltage-division" model and FDTD simulations, bringing two such nanostructures closer should provide higher enhancement values. Gap-dependent FDTD simulations approve this fact and the field enhancement factor exceeds 10^8 for 3 nm gap case.

observed experimentally in the SEM image, beads with a diameter of 20 nm were distributed along pillars using random function. Then a silver toroid is placed on top of the pillar body. Electric field intensity distribution around the silver nanobeads and at the cavity is given in Fig. 4b and c. Positions of the highest electric field enhancement turned out to be inside the bowls as shown in Fig. 4c. Therefore, it is implicitly deduced that bead formation does not influence the enhancement factor. In addition, we demonstrate that nanostructures with an anemone-like cap could provide a greater ($\sim 10^8$) amount of field enhancement compared to bare metal coated nanocylinder geometry ($\sim 10^4$). This behaviour is also reflected when at least two such nanostructures are arranged in close proximity to each other. The total amount of field is further enhanced when structures possess a nanogap, forming the so-called "hot spot". Here the voltage-division model, $\left(\mathrm{EF} \approx \left(\frac{\mathrm{D}}{\mathrm{d}} + 1\right)^4\right)$ where EF is the enhancement factor, D is the diameter of structures and d is the gap (distance), can be used effectively to describe the approximate value of field enhancement for the close nanostructure case. An analogous model can be developed to predict the intensity level of the field within the nanogaps in our case, which as expected will increase when anemone-like nanostructures are closer to each other. We determined that field enhancement significantly increased and reached EF = 10^8 when the gap between nanostructures was as small as 0–3 nm (Fig. 4d and ESI Fig. S6†). We believe the contribution of electromagnetic enhancement can exceed 10^9 for our nanostructure architecture and arrangement, when we consider additional parameters such as curvy behaviour of the anemone cap (where further enhancement may arise due to the gap between modulations). However, it should be noted that precise mechanisms and conceptual underpinnings behind molecule detection *via* Raman Scattering are still speculative and may require alternative approximations and considerations (*e.g.* quantum models) and other contributions such as chemical enhancement.

The SERS performance of nanopillars was demonstrated using Rhodamine 6G (R6G), which is a well-known surface-enhanced Raman dye. The AAO template (periodicity with 120 nm) provides us densely packed nanopillars over a large area. Raman spectra were collected with the 50 μW excitation power at 532 nm. Time dependent spectra were obtained with an integration time of 10 s and averaged spectra were obtained for 10^{-7}, 10^{-9}, and 10^{-12} M R6G on the nanostructured film in Fig. 5. The main Raman active modes of the dye were observed at 610, 777, 1365, 1578, and 1650 cm^{-1} in agreement with previous experimental and theoretical investigations (Fig. 5).[31] The obtained signals at about 1365, 1578, and 1650 cm^{-1} are assigned to symmetric modes of in-plane C–C stretching vibrations. The peak at 777 cm^{-1} is from the out-of-plane bending motion of the hydrogen atoms and the peak at about 610 cm^{-1} corresponds to the C–C–C ring in-plane bending.[32,33] The Raman spectrum slightly shifts at lower concentrations. This phenomenon is explained by chemical enhancement in previous studies.[34] Different concentrations of R6G were used to test the substrate sensitivity and Raman modes were still distinctive even at the picomolar dye concentration. The enhancement factor (EF) was calculated comparing the silver coated nanostructured film and the non-structured bare film at 10^{-12} M and 10^{-3} M R6G dye concentrations, respectively. While the measurements were performed at 50 μW laser power for nanostructured films, the laser power was increased to 40 mW to detect Raman signals on the bare film (ESI Fig. S7†). Anemone-like nanopillars present an EF value of 5.7×10^{11} (detailed calculations are given in ESI.†)

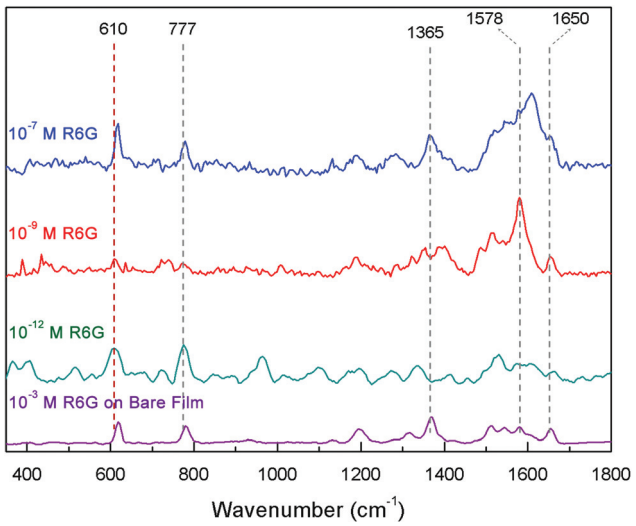

Fig. 5 Surface enhanced Raman spectra and the Raman spectrum. SERS and Raman of R6G on silver coated nanostructured and non-structured polymer films. SERS spectra were collected for 10^{-7}, 10^{-9}, and 10^{-12} M concentrations of R6G by a 532 nm laser source with 50 μW power and main Raman active modes were obtained, shown with dashed lines. Raman spectrum was collected for the 10^{-3} M R6G with higher laser power, which is about 40 mW. Enhancement factor was calculated as 5.7×10^{11} with respect to the peak at ~610 cm^{-1}.

One of the handicaps of SERS sensing is producing stable SERS signals and there is a huge effort to fabricate reliable, reproducible SERS substrates.[35,36] As mentioned before, low reproducibility of the signals can be attributed to the narrow nanogaps or inhomogeneous distribution of the nanostructures or analyte molecules. We tested our densely packed nanostructures to overcome this complication of SERS sensing. In Fig. 6a, SERS spectra were first baseline corrected and then normalized to see the similarity of the measured spectra. Histograms of the main Raman active modes are also given in Fig. 6b–f; these peak distributions were used to determine relative standard deviations (RSDs), which are defined as the ratio of the standard deviation to the mean. We calculated RSDs of the substrate in order to determine the spot-to-spot SERS reproducibility. Calculation was performed for the acquired Raman active modes of the R6G, about 10 000 individual spots were used for the raw data given in ESI Fig. S8.† Map information collected from different regions (5×5 μm^2) of the sample was used at 10^{-7} M concentration with 1 s integration time. As is seen in the confocal microscopy image

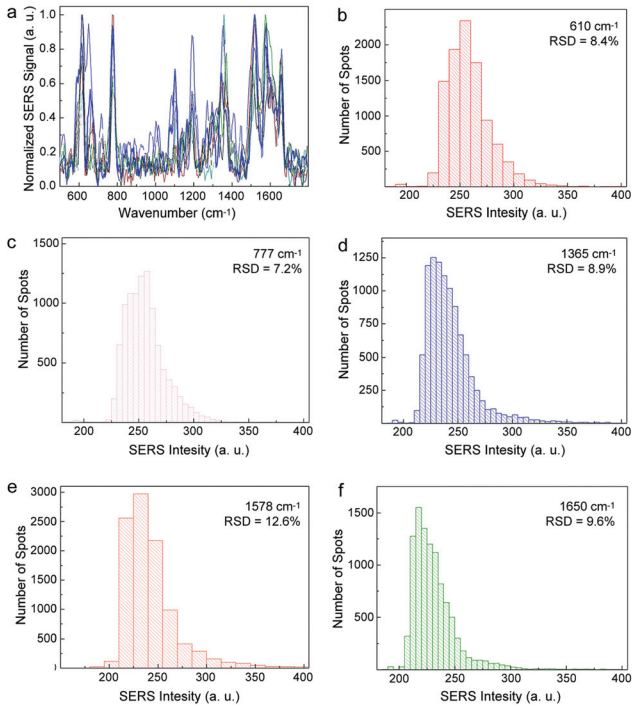

Fig. 6 SERS spectra of R6G on the mapped area for 10 000 spots. (a) Spectra were baseline corrected and normalized to show consistency. (b–f) Histograms of the main Raman modes of R6G are given for 610, 777, 1365, 1578, and 1650 cm^{-1} peaks, respectively. Relative standard deviation (RSD) of the Raman modes was calculated for raw data and varies between 7.2 and 12.6% RSD. Peak distribution and RSD values demonstrate that reproducible SERS signals were detected for the anemone-like nanostructured substrate.

(Fig. S9†), the dried droplet does not have a uniform distribution. Thus, to understand better the working area, the fluorescence intensity was profiled using the ImageJ programme (detailed calculations are given in ESI†). SERS spectra were also consistent for the other concentrations of the R6G. RSDs for the 610, 777, 1365, 1578 and 1650 cm^{-1} peaks were determined as 8.4, 7.2, 9.6, 12.6 and 8.9%, respectively. Distributions show that the measured signals are reproducible and have high precision.

Conclusion

While polymeric nanopillar production is common, here anemone-like nanostructures are produced for the first time under the surface/interface principles of melt-infiltration with a non-lithographic method. This facile and cost-effective production method utilizes reusable templates and overcomes complex environment requirements and multistep fabrication processes. Experimental findings are confirmed by two dimensional numerical FEM simulations using COMSOL and formation of the pillar caps is shown systematically. Fabricated anemone-like nanopillars are examined in SERS media by silver coating. The electric field is localized at the cavity and between the nanopillar caps, as defined by FDTD simulations. We achieved an enhancement factor of $\sim 10^{11}$ at the picomolar level of dye solution. In addition, the spot-to-spot reproducibility of the SERS signals is demonstrated with RSDs of 7.2–12.6%. The obtained results are also promising for biological molecule and single molecule detection platforms. Moreover, the controlled pillar length and cap shape can be utilized in plasmonic substrates, resonators, chemical sensors, or biological applications.

Materials and methods

Fabrication of anemone-like nanostructures

PC anemone-like nanopillars were fabricated using AAO membranes which were produced according to the method mentioned in previous studies.[37] The AAO template was coated with 1% (v/v) 1*H*, 1*H*, 2*H*, 2*H*-perfluorodecyl-trichloro silane (FDTS) in *n*-heptane and cured at 100 °C under vacuum for 1 h. The PC film was placed on the template and heated stepwise to 215 °C. After the sample was cooled to RT, the film was peeled off from the template. Surface characterization of the produced nanopillars was examined using a SEM (Quanta 200 FEG) with a tilt angle of 40°.

Fluid dynamic simulations

Two dimensional numerical finite element method simulations were performed using COMSOL 4.3 for the modeling of heat-mediated nanostructure formation. A level-set function $\phi(x,y,t)$ was coupled with Navier–Stokes (NS) equations for a Newtonian fluid $\rho\left(\frac{du}{dt} + u\cdot\nabla u\right) - \nabla[\eta(\nabla u + \nabla u^{T})] + \nabla p - \gamma\kappa n\delta$, where u is the velocity of an arbitrary point of the fluid, η is the viscosity, p is the pressure, ρ is the density and γ is the interfacial energy.[38–40] The level-set function ϕ was defined as a signed distance function, where the interface between the two fluids was determined by the level-set function at ϕ = 0.5. The normal and curvature were determined from the level set function as $\hat{n} = \frac{\nabla\phi}{|\nabla\phi|}$ and $\hat{k} = -\nabla\frac{\nabla\phi}{|\nabla\phi|}$, respectively. The coupled Navier–Stokes equation and the level-set function were simultaneously solved using the Fluid Dynamics Module in COMSOL.

FDTD simulations

Field enhancement factors and field distribution mapping were calculated with the finite difference time domain technique using the commercial software "Lumerical Solutions". Thicknesses and mesh orders of each compartment were meticulously designed to replicate the original structure. Five of such complete instances were installed in such a way to form the hexagonal lattice with a spacing of 120 nm, and the simulation area was further designed to form a unit cell. As required, simulations were performed in three-dimensional space using periodic boundary conditions, both to decrease

the calculation time and to constitute realistic (ideal) simulations. The light source was set to radiate at a single wavelength of 532 nm based on the Raman laser used in experimental measurements.

To obtain the gap dependent enhancement performance of anemone-like nanostructures two metal-coated toroid structures were used and the gap spacing was tuned between 0 and 15 nm. It was found that especially in smaller gap sizes (*e.g.* 0–3 nm) higher enhancement values could be obtained. The 3D simulation domain and perfectly matched layer (PML) conditions were used to reflect experimental observations appropriately.

SERS measurements

Nanostructured polymer films were coated with a 40 nm silver film by thermal evaporation prior to the measurements. A silver film was deposited at 0.5 A° s^{-1} rate and coating growth was controlled with a thickness monitor. During the deposition step, Ag nanobeads were also formed on the film surface. R6G was used to evaluate the SERS performance of our substrate. Different solutions of R6G were prepared in ethanol at 10^{-7}, 10^{-9}, and 10^{-12} M concentrations and 6 μl of each solution was dropped on the nanopillar decorated substrates. SERS spectra of the samples were collected by exciting with a 532 nm laser source at 50 μW power. For the comparison of nanostructured and non-structured surfaces, a bare PC film was coated with silver under the same conditions. 6 μl of 10^{-3} M R6G solution was drop cast on the bare film and the Raman spectrum was collected at 40 mW. The enhancement factor was calculated comparing the dye solutions at 10^{-12} M and 10^{-3} M concentrations for nanostructured and bare films, respectively (calculation details are given in ESI†).

Acknowledgements

This work was supported by the TUBITAK grant no. 111T696. M. B. acknowledges partial support from the Turkish Academy of Sciences (TUBA).

Notes and references

1 P. E. De Jongh and T. M. Eggenhuisen, *Adv. Mater.*, 2013, **25**, 6672.
2 H. Izadi, M. Golmakani and A. Penlidis, *Soft Matter*, 2013, **9**, 1985.
3 J. Martin and C. Mijangos, *Langmuir*, 2009, **25**, 1181.
4 M. Steinhart, R. B. Wehrspohn, U. Gosele and J. H. Wendorff, *Angew. Chem., Int. Ed.*, 2004, **43**, 1334.
5 C. A. Huber, T. E. Huber, M. Sadoqi, J. A. Lubin, S. Manalis and C. B. Prater, *Science*, 1994, **263**, 800.
6 S. I. Moon and T. J. McCarthy, *Macromolecules*, 2003, **36**, 4253.
7 T. M. Eggenhuisen, J. P. den Breejen, D. Verdoes, P. E. de Jongh and K. P. de Jong, *J. Am. Chem. Soc.*, 2010, **132**, 18318.
8 G. B. Demirel, F. Buyukserin, M. A. Morris and G. Demirel, *ACS Appl. Mater. Interfaces*, 2012, **4**, 280.
9 S. M. Jeon, Y. Lee, J. H. Kim, J. K. Lee, K. Char and B. H. Sohn, *React. Funct. Polym.*, 2009, **69**, 558.
10 J. Lee, J. Kim and T. Hyeon, *Adv. Mater.*, 2006, **18**, 2073.
11 B. Platschek, A. Keilbach and T. Bein, *Adv. Mater.*, 2011, **23**, 2395.
12 E. V. Skorb and D. V. Andreeva, *Adv. Funct. Mater.*, 2013, **23**, 4483.
13 B. Daglar, T. Khudiyev, G. B. Demirel, F. Buyukserin and M. Bayindir, *J. Mater. Chem. C*, 2013, **1**, 7842.
14 N. Ji, W. Ruan, Z. Li, C. Wang, Z. Yang and B. Zhao, *J. Raman Spectrosc.*, 2013, **44**, 1.
15 K. Sun, G. Meng, Q. Huang, X. Zhao, C. Zhu, Z. Huang, Y. Qian, X. Wanga and X. Hua, *J. Mater. Chem. C*, 2013, **1**, 5015.
16 A. Virga, P. Rivolo, F. Frascella, A. Angelini, E. Descrovi, F. Geobaldo and F. Giorgis, *J. Phys. Chem. C*, 2013, **117**, 20139.
17 H. Ko, S. Singamaneni and V. V. Tsukruk, *Small*, 2008, **4**, 1576.
18 E. Ringe, B. Sharma, A. I. Henry, L. D. Marks and R. P. Van Duyne, *Phys. Chem. Chem. Phys.*, 2013, **15**, 4110.
19 M. Zhang, A. Zhao, H. Sun, H. Guo, D. Wang, D. Li, Z. Gan and W. Tao, *J. Mater. Chem.*, 2011, **21**, 18817.
20 H. Wei and H. Xu, *Nanoscale*, 2013, **5**, 10794.
21 J. D. Caldwell, O. Glembocki, F. J. Bezares, N. D. Bassim, R. W. Rendell, M. Feygelson, M. Ukaegbu, R. Kasica, L. Shirey and C. Hosten, *ACS Nano*, 2011, **5**, 4046.
22 S. Habouti, M. Matefi-Tempfli, C.-H. Solterbeck, M. Es-Souni, S. Matefi-Tempfli and M. Es-Souni, *Nano Today*, 2011, **6**, 12.
23 F.I. Dar, S. Habouti, R. Minch, M. Dietze and M. Es-Souni, *J. Mater. Chem.*, 2012, **22**, 8671.
24 J. A. Huang, Y. Q. Zhao, X. J. Zhang, L. F. He, T. L. Wong, Y. S. Chui, W. J. Zhang and S. T. Lee, *Nano Lett.*, 2013, **13**, 5039.
25 D. Schebarchov and S. C. Hendy, *Nano Lett.*, 2008, **8**, 2253.
26 W. Y. Chang, K. H. Lin, J. T. Wu, S. Y. Yang, K. L. Lee and P. K. Wei, *J. Micromech. Microeng.*, 2011, **21**, 035023.
27 D. G. Legrand and J. T. Bendler, *Handbook of Polycarbonate Science and Technology*, CRC Press, New York, USA, 2000.
28 F. Yang, *Polym. Eng. Sci.*, 1997, **37**, 101.
29 J. Brandrup and E. H. Immergut, *Polymer Handbook*, Wiley, New York, USA, 1989.
30 D. I. Dimitrov, A. Milchev and K. Binder, *Phys. Rev. Lett.*, 2007, **99**, 054501.
31 J. A. Dieringer, K. L. Wustholz, D. J. Masiello, J. P. Camden, S. L. Kleinman, G. C. Schatz and R. P. Van Duyne, *J. Am. Chem. Soc.*, 2009, **131**, 849.
32 S. Nie and S. R. Emory, *Science*, 1997, **275**, 1102.

33 M. Yi, D. Zhang, P. Wang, X. Jiao, S. Blair, X. Wen, Q. Fu, Y. Lu and H. Ming, *Plasmonics*, 2011, **6**, 515.
34 P. Hildebrandt and M. Stockburger, *J. Phys. Chem.*, 1984, **88**, 5935.
35 N. G. Greeneltch, M. G. Blaber, A.-I. Henry, G. C. Schatz and R. P. Van Duyne, *Anal. Chem.*, 2013, **85**, 2297.
36 A. C. De Luca, P. Reader-Harris, M. Mazilu, S. Mariggio, D. Corda and A. Di Falco, *ACS Nano*, 2014, **8**, 2575.
37 F. Buyukserin, M. Aryal, J. Gao and W. Hu, *Small*, 2009, **5**, 1632.
38 E. Olsson and G. Kreiss, *J. Comput. Phys.*, 2005, **210**, 225.
39 B. Chinè and M. Monno, Proc. COMSOL Conference, Boston, USA, 2010.
40 D. Conchouso, E. Rawashdeh, A. Arevalo, D. Castro and I. G. Foulds, Proc. COMSOL Conference, 2013.